

A new class of Hanbury-Brown/Twiss parameters

Urs Achim Wiedemann and Ulrich Heinz
Institut für Theoretische Physik, Universität Regensburg,
D-93040 Regensburg, Germany
 (September 6, 2018)

In heavy ion collisions resonances can create strong non-Gaussian effects in the 2-pion correlation data. Hence, the commonly used Gaussian fit parameters do not fully characterize these correlators. We suggest a different set of HBT parameters which does not presuppose a particular shape of the correlator and allows to extract additional (non-Gaussian) information. Within a simple model for an expanding source including resonance decays it is shown that this additional information provides a clean distinction between scenarios with and without transverse flow.

PACS numbers: 25.75.+r, 07.60.ly, 52.60.+h

The aim of Hanbury-Brown/Twiss (HBT) interferometric analyses of heavy ion collisions is to extract from the measured 2-particle correlators $C(\mathbf{q}, \mathbf{K})$ of identical particles as much information as possible about the spatio-temporal distribution $S(x, K)$ of the particle emitting sources in the collision region. It is based on the relation [1,2]

$$C(\mathbf{p}_1, \mathbf{p}_2) = 1 + \frac{|\int d^4x S(x, K) e^{iq \cdot x}|^2}{|\int d^4x S(x, K)|^2},$$

$$q = p_1 - p_2, \quad K = \frac{1}{2}(p_1 + p_2). \quad (1)$$

So far, the interplay between the experimentally measurable momentum correlator $C(\mathbf{q}, \mathbf{K})$ and the theoretical concept of space-time emission function $S(x, K)$ was investigated mainly in the context of Gaussian approximations for both. Experimental data are commonly fit to a Gaussian ansatz [3]

$$C(\mathbf{q}, \mathbf{K}) = 1 + \lambda(\mathbf{K}) e^{-q_i q_j R_{ij}^2(\mathbf{K})}, \quad (2a)$$

$$R_{ij}(\mathbf{K}) = \begin{pmatrix} R_{oo}^2 & R_{os}^2 & R_{ol}^2 \\ R_{os}^2 & R_s^2 & R_{sl}^2 \\ R_{ol}^2 & R_{sl}^2 & R_l^2 \end{pmatrix}, \quad i, j = o, s, l. \quad (2b)$$

Here, the relative momentum components are defined parallel to the beam ($l = longitudinal$), parallel to the transverse component of \mathbf{K} ($o = out$), and in the remaining third direction ($s = side$). $R_{os} = R_{sl} = 0$ for azimuthally symmetric collisions.

The fit parameters $R_{ij}^2(\mathbf{K})$ can be calculated from a Gaussian ansatz for the emission function $S(x, K)$ in terms of space-time variances $\langle \tilde{x}_\mu \tilde{x}_\nu \rangle$ [4,5]:

$$S(x, K) \simeq N(K) S(\bar{x}, K) e^{-\frac{1}{2} \tilde{x}^\mu \tilde{x}^\nu B_{\mu\nu}(\mathbf{K})}, \quad (3a)$$

$$(B^{-1})_{\mu\nu} = \langle \tilde{x}_\mu \tilde{x}_\nu \rangle, \quad \tilde{x}_\mu = x_\mu - \bar{x}_\mu, \quad \bar{x}_\mu = \langle x_\mu \rangle, \quad (3b)$$

$$\langle f(x) \rangle = \langle f(x) \rangle(K) = \frac{\int d^4x f(x) S(x, K)}{\int d^4x S(x, K)}. \quad (3c)$$

In the resulting expression for the correlator,

$$C(\mathbf{q}, \mathbf{K}) = 1 + \exp(-q^\mu q^\nu \langle \tilde{x}_\mu \tilde{x}_\nu \rangle), \quad (4)$$

only three of the four relative momentum components are independent, the fourth being fixed via the on-shell constraint $q^0 = \mathbf{q} \cdot (\mathbf{K}/K^0) = \mathbf{q} \cdot \boldsymbol{\beta}$. In the Gaussian framework, the consequences of the on-shell constraint are well studied. Especially, the HBT radius parameters read [3,6]

$$R_{ij}^2(\mathbf{K}) = \langle (\tilde{x}_i - \beta_i \tilde{t})(\tilde{x}_j - \beta_j \tilde{t}) \rangle. \quad (5)$$

This is the starting point of most spatio-temporal interpretations of correlation data. Note however that (6) presupposes a Gaussian shape of $C(\mathbf{q}, \mathbf{K})$ since (6) determines the curvature components of the correlator at $\mathbf{q} = 0$ [3]:

$$R_{ij}^2(\mathbf{K}) = - \left. \frac{\partial^2 C(\mathbf{q}, \mathbf{K})}{\partial q_i \partial q_j} \right|_{\mathbf{q}=0}, \quad (6)$$

and these coincide with the experimentally determined half widths of $C(\mathbf{q}, \mathbf{K})$ only for Gaussian correlators. Non-Gaussian characteristics of the correlator are difficult to quantify and control in this Gaussian framework.

Here, we suggest to characterize the correlator with a different set of a few HBT parameters, so-called q -moments, whose extraction does not presuppose a particular shape of $C(\mathbf{q}, \mathbf{K})$.

The HBT parameters used in the Gaussian framework are based on space-time variances $\langle \tilde{x}_\mu \tilde{x}_\nu \rangle$, i.e. on expectation values $\langle f(x) \rangle$ of the emission function in coordinate space, cf. (3c). In contrast, we suggest here to base a quantitative analysis of $C(\mathbf{q}, \mathbf{K})$ on q -variances which are expectation values $\langle\langle g(\mathbf{q}) \rangle\rangle$ of the true correlator $C(\mathbf{q}, \mathbf{K}) - 1$ in relative momentum space.

For a Gaussian correlator, the HBT parameters can be determined either by fitting to the Gaussian (2), or by computing the integrals

$$\langle\langle q_i q_j \rangle\rangle = \frac{\int d^3q q_i q_j [C(\mathbf{q}, \mathbf{K}) - 1]}{\int d^3q [C(\mathbf{q}, \mathbf{K}) - 1]} = \frac{1}{2} (R^{-1}(\mathbf{K}))_{ij}, \quad (7)$$

$$\lambda = \sqrt{\det R(\mathbf{K})/\pi^3} \int d^3q [C(\mathbf{q}, \mathbf{K}) - 1]. \quad (8)$$

For a non-Gaussian correlator, we can *define* the HBT radius parameters and the intercept λ in terms of these “ q -variances”.

The deviations of the correlator from a Gaussian shape (“non-Gaussianities”) are then quantified by higher order q -moments. Due to the $\mathbf{q} \rightarrow -\mathbf{q}$ symmetry of $C(\mathbf{q}, \mathbf{K})$ the first non-Gaussian contribution shows up in the fourth order q -moments (“kurtosis”). All higher order q -moments can be calculated as derivatives of the generating function $Z(\mathbf{y}, \mathbf{K})$,

$$Z(\mathbf{y}, \mathbf{K}) = \int d^3q e^{i\mathbf{q}\cdot\mathbf{y}} [C(\mathbf{q}, \mathbf{K}) - 1], \quad (9)$$

$$\langle\langle q_{i_1} q_{i_2} \dots q_{i_n} \rangle\rangle = (-i)^n \frac{\partial^n}{\partial y_{i_1} \partial y_{i_2} \dots \partial y_{i_n}} \ln Z(\mathbf{y}, \mathbf{K}) \Big|_{\mathbf{y}=0}. \quad (10)$$

From this generating function, the correlator can be reconstructed completely. The series of n -th q -variances (10) is merely a convenient way to characterize its shape starting with its “Gaussian” widths $\langle\langle q_i q_j \rangle\rangle$ and going for increasing n step by step to finer structures.

To calculate $Z(\mathbf{y}, \mathbf{K})$ directly from a given emission function it is convenient to use the normalized “relative distance distribution”

$$\begin{aligned} \rho(u; K) &= \int d^4X s(X + \frac{u}{2}, K) s(X - \frac{u}{2}, K), \\ \int d^4u \rho(u; K) &= 1, \end{aligned} \quad (11)$$

written in terms of the normalized emission function $s(x, K) = S(x, K) / \int d^4x S(x, K)$. ρ is real and even in u . Then

$$Z(\mathbf{y}, \mathbf{K}) = \int d^3q e^{i\mathbf{q}\cdot\mathbf{y}} \int d^4u e^{iq\cdot u} \rho(u; K). \quad (12)$$

In the Cartesian parametrization, this expression simplifies to a one-dimensional integral:

$$Z(\mathbf{y}, \mathbf{K}) = \int dt \rho(y_s, y_o + \beta_\perp t, y_l + \beta_l t, t; K). \quad (13)$$

For Gaussian emission functions Eqs. (7), (10) and (13) reproduce the relations (5).

The method of q -variances generally requires to invert the matrix (7) and to discuss a 4-dimensional tensor of fourth order moments. Such a full analysis will be published elsewhere [7]. Here, we restrict ourselves to a unidirectional analysis of the correlations $\tilde{C}(q_i, \mathbf{K}) \equiv C(q_i, q_{j \neq i} = 0, \mathbf{K})$ along the three Cartesian axes. For the relative momentum component q_i , the corresponding HBT radius parameter and intercept are then defined via the relations (we use the same notation as for the three-dimensional q -moments)

$$R_i^2(\mathbf{K}) = \frac{1}{2 \langle\langle q_i^2 \rangle\rangle}, \quad (14a)$$

$$\langle\langle q_i^2 \rangle\rangle = \frac{\int dq_i q_i^2 [\tilde{C}(q_i, \mathbf{K}) - 1]}{\int dq_i [\tilde{C}(q_i, \mathbf{K}) - 1]}, \quad (14b)$$

$$\lambda_i(\mathbf{K}) = (R_i(\mathbf{K}) / \sqrt{\pi}) \int dq_i [\tilde{C}(q_i, \mathbf{K}) - 1]. \quad (14c)$$

Even Gaussian correlators have non-vanishing higher q -moments:

$$\langle\langle q_i^{2m} \rangle\rangle^{\text{Gauss}} = \frac{(2m-1)!!}{(2R_i^2)^m}. \quad (15)$$

Being expressible in terms of the second moments they do not contain new information. The non-trivial higher order information is contained in the (normalized) q -cumulants, in which these trivial contributions are subtracted:

$$\Delta_i^{(2m)} = \frac{1}{(2m-1)!!} \frac{\langle\langle q_i^{2m} \rangle\rangle}{\langle\langle q_i^2 \rangle\rangle^m} - 1. \quad (16)$$

The normalization removes the dependence on the Gaussian widths of $C(\mathbf{q}, \mathbf{K})$ and turns them into dimensionless measures for deviations from a Gaussian shape.

To extract the moments $\langle\langle q_i^n \rangle\rangle$ from data one replaces (14b) by a ratio of sums over bins in the q_i -direction. The higher the order n of the q -moment, the more sensitive are the extracted values to statistical and systematic uncertainties in the region of large q_i . First investigations with event samples generated by the VENUS event generator indicate that the current precision of the data in the Pb-beam experiments at the CERN SPS permits to determine the second and fourth order q -moments [7]. Accordingly, we restrict our discussion of non-Gaussian features to the “kurtosis”

$$\Delta_i = \frac{\langle\langle q_i^4 \rangle\rangle}{3 \langle\langle q_i^2 \rangle\rangle^2} - 1. \quad (17)$$

We have computed the unidirectional Gaussian parameters R_i and the kurtosis Δ_i for a model pion emission function including resonance decay channels R :

$$S_\pi(x, p) = S_\pi^{\text{dir}}(x, p) + \sum_R S_{R \rightarrow \pi}(x, p). \quad (18)$$

The contributions $S_{R \rightarrow \pi}$ are obtained from the direct resonance emission function $S_R^{\text{dir}}(X, P)$ by propagating the resonances of widths Γ , produced at (X_μ, P_μ) , along a classical path $x^\mu = X^\mu + \frac{P^\mu}{M} \tau$ according to an exponential decay law [8,9]:

$$\begin{aligned} S_{R \rightarrow \pi}(x; p) &= M \int_{s_-}^{s_+} ds g(s) \int \frac{d^3P}{E_P} \delta(P \cdot p - ME^*) \\ &\times \int d^4X \int d\tau \Gamma e^{-\Gamma\tau} \delta^{(4)}(x - (X + \frac{P}{M}\tau)) \\ &\times S_R^{\text{dir}}(X, P). \end{aligned} \quad (19)$$

We consider isotropic decays in the resonance rest frame with decay phase space $g(s)$, E^* being the energy of the

observed decay pion in this frame and s the squared invariant mass of the $(n-1)$ unobserved decay products.

Our model assumes local thermalization at freeze-out and produces hadronic resonances by thermal excitation. For particle species i with spin degeneracy $2J_i + 1$, the emission function reads [4]

$$S_i^{\text{dir}}(x, P) = \frac{2J_i+1}{(2\pi)^3} P \cdot n(x) \exp\left(-\frac{P \cdot u(x) - \mu_i}{T}\right) H(x),$$

$$H(x) = \exp\left(-\frac{r^2}{2R^2} - \frac{\eta^2}{2(\Delta\eta)^2} - \frac{(\tau - \tau_0)^2}{2(\Delta\tau)^2}\right). \quad (20)$$

The Boltzmann factor $\exp[-(P \cdot u(x) - \mu_i)/T]$ implements both the assumption of thermalization, with temperature T and chemical potential μ_i , and collective expansion with hydrodynamic flow 4-velocity $u_\mu(x)$. Space-time is parametrized via longitudinal proper time $\tau = \sqrt{t^2 - z^2}$, space-time rapidity $\eta = \frac{1}{2} \ln[(t+z)/(t-z)]$, transverse radius r and azimuthal angle ϕ . The Gaussian factors in $H(x)$ specify the spatial extension of the source as well as a Gaussian average around a mean freeze-out proper time τ_0 with dispersion $\Delta\tau$. For freeze-out along proper time hyperbolae $P \cdot n(x) = M_\perp \cosh(Y - \eta)$ [4] where Y and M_\perp are the rapidity and transverse mass associated with P .

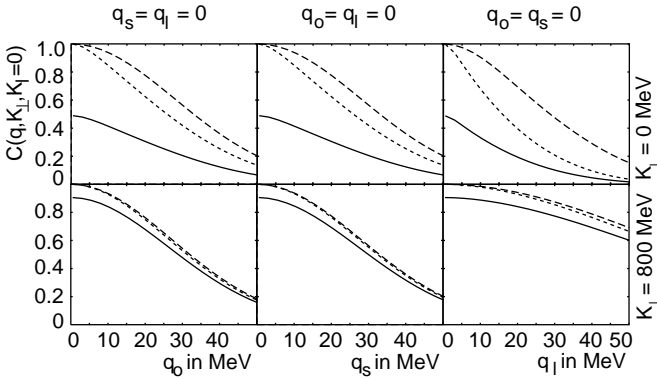


FIG. 1. Two-pion correlations for transverse flow $\eta_f = 0$. Curves are calculated for the model emission function (20) without resonance decay contributions (dashed lines), including pions from the shortlived resonances ρ , Δ , K^* , Σ^* and from the ω (dotted lines), and including also pions from the longlived resonances η , η' , K_S^0 , Σ , Λ (solid lines).

In the longitudinal direction we assume scaling expansion, $v_l = z/t$ or $\eta_l = \frac{1}{2} \ln[(1+v_l)/(1-v_l)] = \eta$. For the transverse expansion we choose a linear rapidity profile:

$$\eta_t(r) = \eta_f \left(\frac{r}{R}\right). \quad (21)$$

All numerical results presented here are obtained for the set of source parameters $T = 150$ MeV, $R = 5$ fm, $\Delta\eta = 1.2$, $\tau_0 = 5$ fm/c, $\Delta\tau = 1$ fm/c and $\mu_B = \mu_S = 0$. We include all pion decay channels of ρ , Δ , K^* , Σ^* , ω ,

η , η' , K_S^0 , Σ and Λ with branching ratios larger than 5 percent [10].

For this model we have numerically computed the 2-pion correlator. Typical results are shown in Fig. 1. A detailed model study of how resonance contributions affect the shape and pair momentum dependence of the correlator will be published elsewhere [11]. Here, we merely observe that due to their exponential decay law, resonance decays can contribute exponential tails to the emission function $S_{R \rightarrow \pi}$ in (19), thereby leading to a generically non-Gaussian shape of the correlator.

To illustrate the use of q -variances we now discuss how the space-time characteristics of the emission region, specified in our model by the geometric input parameters and the transverse flow η_f , show up in these new 2-particle observables. First, we checked that for the model (18-20) the inverted second q -moments R_i coincide in all three directions $i = 0, s, l$ with the Gaussian fit parameters extracted for a set of n equidistant points $q_i^{(j)}$ between 0 and 50 MeV by minimizing

$$\sum_{j=1}^n \left(\ln \tilde{C}(q_i^{(j)}, \mathbf{K}) - \log \lambda + R_i^2 q_i^{(j)2} \right) = \min. \quad (22)$$

These ‘‘Gaussian’’ radius parameters R_i and their transverse momentum dependence is well-studied for model emission functions (20) not including resonance decay contributions [5]. Especially, it is known that the transverse homogeneity length R_t of (20), i.e. the size of the effective emission region in the transverse plane, shrinks with transverse flow η_f approximately like [5]

$$R_t \approx R \left(1 + \frac{M_\perp}{T} \eta_f^2 \right)^{-\frac{1}{2}}. \quad (23)$$

This introduces an η_f -dependent K_\perp -slope of R_s which was interpreted previously as a signature of transverse flow. Fig. 2 shows that if resonance decay contributions are added in the calculation, this distinctive behaviour is lost: R_s develops a K_\perp -slope even for scenarios without transverse flow. The reason is that resonances can propagate outside of the thermally equilibrated region before decaying. This effect (‘‘lifetime effect’’) leads to exponential tails in $S_{R \rightarrow \pi}$ and tends to increase the Gaussian widths R_i . Since the relative abundance of resonances is larger for small K_\perp , this tail is more pronounced in the region of small K_\perp , thereby leading to a K_\perp -slope of R_s .

In contrast, for a finite transverse flow $\eta_f = 0.3$ the K_\perp -dependence of R_s is due to the flow, and resonance decay contributions do not change the slope of R_s in our model. This can be traced back to the shrinking transverse size (23) of the direct resonance emission function S_R^{dir} in (20): due to their larger rest mass, parent resonances have a smaller effective emission region than thermal pions in the transverse direction. For the case depicted in Fig. 2, this effect counterbalances the lifetime effect almost exactly.

According to (23), the absolute size of the *side* radius depends not only on η_f but also on the input parameter R for which no independent measurement exists. As a consequence, the Gaussian radius parameter $R_s(K_\perp)$ by itself does not allow to distinguish scenarios with and without transverse flow once resonance decays are included. This conclusion extends to the other Gaussian widths, R_o and R_l , as well.

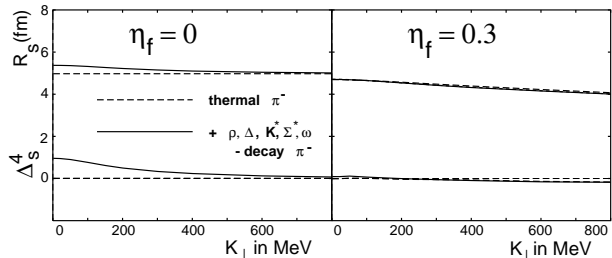


FIG. 2. The inverted q -variance R_s of (2.8a) and the kurtosis Δ_s of (2.11) in the side direction at $Y = 0$ as functions of K_\perp . Left: $\eta_f = 0$ (no transverse flow). Right: $\eta_f = 0.3$. The difference between the dashed and solid curves is entirely dominated by ω decays.

However, the physical origin of the K_\perp -slope of R_s is different for the two situations shown in Fig. 2. This shows up in the kurtosis of the corresponding correlators: without transverse flow, resonance decay contributions increase R_s due to the lifetime effect which generates exponential tails in $S_{R \rightarrow \pi}$. These tails manifest themselves in the correlator through a significant non-Gaussian component. For non-zero transverse flow, on the other hand, the K_\perp -slope arises from the K_\perp -dependent shrinking (23) of the effective transverse emission region. This effect is more prominent for resonances than for thermal pions, i.e. S_π^{dir} is spatially more extended in the transverse plane than S_R^{dir} , and hence it “covers” a substantial part of the exponential tails of $S_{R \rightarrow \pi}$. As a consequence, the total emission function (18) can be expected to show much smaller deviations from a Gaussian shape for the scenario with transverse flow, and this again leads to a more Gaussian correlator.

This explains why the kurtosis $\Delta_s(K_\perp)$ plotted in Fig. 2 provides a clearcut distinction between the two scenarios. Δ_s simply reflects the importance of resonance decays. For vanishing transverse flow, Δ_s is significant and decreases with increasing K_\perp since the relative abundance of resonance decay pions dies out; for finite transverse flow $\eta_f = 0.3$, it is an order of magnitude smaller. A K_\perp -dependence of R_s without measurable kurtosis is thus a clear sign of transverse flow.

Here, we do not discuss to what extent this particular η_f -dependence of the kurtosis Δ_s is generic for realistic models of heavy ion collisions including resonance decays. This will require a more systematic study [11]. We simply conclude that higher order q -variances can provide cru-

cial additional information on the correlator which can help to distinguish physical scenarios which are difficult to disentangle on the level of “Gaussian” HBT radius parameters. On the other hand, they can still be directly related to specific features of the emission function and thus should aid the spatio-temporal interpretation of correlation measurements. This is less straightforward if one only knows the overall shape of the correlator, without decomposing it into its moments.

In summary, we expect these new HBT parameters, both the one- and multi-dimensional q -moments of the correlator, to become valuable additional observables in future comparisons between models and experiment.

This work was supported by BMBF, DFG and GSI. Discussions with P. Foka, H. Kalechofsky, B. Lasiuk, M. Martin, H.-P. Naef, L. Rosselet, P. Seyboth and S. Voloshin are gratefully acknowledged.

-
- [1] E. Shuryak, Phys. Lett. B**44**, 387 (1973); Sov. J. Nucl. Phys. **18**, 667 (1974).
 - [2] S. Chapman and U. Heinz, Phys. Lett. B**340**, 250 (1994).
 - [3] S. Chapman, P. Scotto and U. Heinz, Phys. Rev. Lett. **74**, 4400 (1995); and Heavy Ion Phys. **1**, 1 (1995).
 - [4] S. Chapman, J.R. Nix and U. Heinz, Phys. Rev. C**52**, 2694 (1995).
 - [5] U.A. Wiedemann, P. Scotto and U. Heinz, Phys. Rev. C**53**, 918 (1996).
 - [6] M. Herrmann and G.F.Bertsch, Phys. Rev. C**51** (1995), 328.
 - [7] P. Foka, H. Kalechofsky and U.A. Wiedemann, in preparation.
 - [8] P. Grassberger, Nucl. Phys. B**120**, 231 (1977).
 - [9] B.R. Schlei et al., Phys. Lett. B**293**, 275 (1992); J. Bolz et al., Phys. Lett. B**300**, 404 (1993); and Phys. Rev. D**47**, 3860 (1993).
 - [10] Particle Data Book, Phys. Rev. D**50**, 1173 (1994).
 - [11] U.A. Wiedemann and U. Heinz, preprint TPR-96-14.